Materials Science and Engineering A 500 (2009) 207–215

Contents lists available at ScienceDirect

Materials Science and Engineering A

journal homepage: www.elsevier.com/locate/msea

On the origin of the stress decrease for nickel polycrystals with few grains across the thickness

C. Keller, E. Hug*, D. Chateigner

Laboratoire de Cristallographie et Sciences des Matériaux, ENSICAEN, Université de Caen, CNRS, 6 Bd Maréchal Juin, F-14050 Caen 4, France

ARTICLE INFO

Article history:
Received 4 February 2008
Received in revised form 9 September 2008
Accepted 12 September 2008

Keywords:
Nickel
Size effect
Grain size
Microstructure
Hall–Petch law

ABSTRACT

The mechanical behaviour under uniaxial and loading/unloading tensile tests of high purity nickel with different number of grains across the thickness is studied experimentally. The specimens have a constant 500 μm thickness and the mean number of grains across the thickness (i.e., thickness "*t*" to grain size "*d*" ratio) lies between 0.9 and 15. An extended microstructural study is operated and no change of the microstructure appears with a modification of *t*/*d*. The experimental results show that the *t*/*d* ratio affects the hardening stages, flow stress, intragranular and intergranular backstress of the samples. For specimens with few grains across the thickness, the flow stress is reduced due to a decrease in the intragranular backstress. The main explanation of these results is a delay of the generalization of cross-slip for the lowest *t*/*d* ratio specimens due to surface effects.

1. Introduction

As a result of the trend of miniaturization on medical, electrical or mechanical devices, the industrial need for micrometal parts has increased since 1990s. Today, thin films or plates are mass produced and processed. As the thickness is reduced, the free surfaces and the size effects become dominant and the continuum mechanics validity may be lost. These three "size" effects: thickness (*t*) to grain size (*d*) ratio, free surface and dimension effects are correlated and difficult to analyse separately. Nevertheless, in order to simulate the forming process accurately, appropriate models and constitutive laws for such small dimensions are of prime importance. Active experimental research on thin sheets is therefore necessary to understand the mechanical behaviour and to improve the forming process and the reliability of such devices.

During 1960s, 1970s and 1980s, free surface and thickness effects were widely studied using mechanical tests and TEM investigations on Cu and Al single crystals [1–8]. A decrease of stress near the free surfaces and a modification of the hardening stages with a reduction of the thickness for samples with no oxide surface layer were reported [1–7]. Mechanisms based on activated glide systems were also enounced [1,5]. The extension of the study on polycrystals was difficult and only a few works deal with these size effects [9–13]. For polycrystals, it was found for Cu, Al and Ni that the free surfaces have a similar influence to that of single crystals [9,10,13].

The effect of the *t*/*d* ratio was first pointed out during 1960s by Armstrong [14] and Thompson [15]. Since 1970s, several studies on Al and Cu have shown that mechanical properties of polycrystals are modified by a decrease in the number of grains across the thickness below a critical value. This latter seems to depend on stacking fault energy and grain size [16]. The main feature is a decrease in the flow stress for the lowest *t*/*d* ratio specimens [16–21]. It was also reported that the critical *t*/*d* ratio for nickel depends on the strain level and that the Hall–Petch coefficients are modified when *t*/*d* is lower than the critical value [22]. At the same time, due to the ongoing demand of manufactured small devices, several studies were carried out on industrial alloys to investigate the *t*/*d* effect on material processing [23–26]. A modification of the mechanical properties and a decrease of the formability of thin metal sheets with a decrease of *t*/*d* were found [23,26]. Results from both the experimental and processing communities are in agreement.

The common explanation for the modification of mechanical properties for samples with few grains across the thickness is that surface grains are less constrained than core grains [15,16,18,19,23,24,27]. As the *t*/*d* ratio decreases, surface grains become dominant and the overall mechanical behaviour is modified. However, the mechanisms responsible for the behaviour difference between surface and core grains have not been fully described and still need more investigation.

In order to conclude about the *t*/*d* effect, special attention has to be paid to the following features. First, the complexity of the

* Corresponding author. Tel.: +33 2 31 45 13 13; fax: +33 2 31 95 16 00.
E-mail address: eric.hug@ensicaen.fr (E. Hug).

0921-5093/$ – see front matter © 2008 Elsevier B.V. All rights reserved.
doi:10.1016/j.msea.2008.09.054

microstructure giving rise to various deformation mechanisms could bias our understanding of the mechanisms occurring with a decrease of t/d. Choosing a simple face centred cubic metal with high stacking fault energy is therefore suitable for an easier interpretation. In such metals, the deformation mechanisms are understood. Secondly, an extensive investigation of the microstructure is necessary. As pointed out recently by Janssen et al. [18], preparing specimens with different t/d ratios induces a serious risk of differences occuring in crystallographic texture and oxide layer formation. These differences may cause serious modifications of the mechanical properties which can impede the analysis of the size effects. For example, Nemat-Nasser et al. [28] reported numerically different stress levels for specimens with a variation of the grain orientation across the thickness. Thirdly, the different size effects described above have to be studied separately. In some studies, the t/d ratio is varied by a modification of the thickness and the grain size jointly, making the separation of the two effects difficult.

The purpose of this paper is first to study the t/d ratio effect on high purity nickel (99.98%). Nickel has a high stacking fault energy (125 mJ/m^2) intermediate between aluminium (135 mJ/m^2) and copper (45 mJ/m^2). Comparisons with these latter can therefore shed light on the t/d effect. The second objective is to carry out an extended study of nickel microstructure as a function of grain size and t/d ratio in order to exclude any effect of this latter on the mechanical behaviour. Thirdly, the aim is to try to decorrelate the grain size and t/d ratio effects on the mechanical behaviour by studying the modification of Hall–Petch law for specimens of constant thickness. So the overall ambition is to propose a mechanism responsible for the decrease of the flow stress for specimens with few grains across the thickness.

2. Material study and experimental procedure

2.1. Specimen elaboration

Dog bone shape samples of nickel were machined from 0.5-mm rolled sheets for tensile test experiments. The specimens were cut parallel to the original rolling direction of the sheets with gauge dimensions of 70 mm in length and 12 mm in width.

Different grain sizes were required to vary the number of grains across the thickness (this latter being kept constant to 0.5 mm). The samples were annealed in secondary vacuum during 220 min at temperatures between 873 K and 1323 K and then air cooled to modify the grain size. The use of secondary vacuum during the heat treatment is very important for surface effect considerations. The presence of an oxide layer on the surface was found to prevent dislocation escape through the surface [8]. The mechanical behaviour is therefore modified by the formation of a hard layer near the surface as shown particulary for Al [8]. In this study, using secondary vacuum with a partial pressure of O_2 of 2×10^{-11} bar, no oxide layer was found on nickel samples after the heat treatment. Furthermore, the cutting process induces a modification of the microstructure near the cut edges which can lead to a processing induce size effect [29]. The secondary recrystallization event which takes place during the heat treatment allows the annihilation of the affected microstructure near the cut edges and homogenises the latter, especially for the high temperature treatments.

2.2. Specimen characterization

Mean grain size, crystallographic texture, elastic properties and grain boundary character distribution were analysed.

The mean grain size was calculated by numerical treatment of surface images of the sample. The surface was first electropolished (A2 Struers® electrolyte) and chemically etched by a Marble solution (ethanol + HCl + $CuSO_4$). Secondly, an image analysis reported the mean area for each grain of the sample. A mean volumetric grain size is therefore calculated from all the surface grains ranging between 33 μm and 530 μm. No differentiation between surface grain size and volumetric grain size was applied. The surface grain size definition is appropriate for samples with less than one grain across the thickness [18]. In this study, the samples have at least one grain across the thickness with generally only one free surface. Consequently, in order to simplify the grain size formulation, we have used a volumetric grain size for all samples. A typical standard deviation for the grain size around half this latter was found for each specimen. A large standard deviation value is expected to modify the mechanical behaviour of specimens exhibiting a grain size lower than 2 μm, as numerically shown by Berbenni et al. [30]. For larger grain sizes, this effect is considerably reduced. In consequence, we assume that for all the specimens, the standard deviation has no influence on the mechanical properties. The number of grains across the thickness varies from 0.9 to 15. Table 1 reports an example of six heat treatment conditions and the obtained grain size, standard deviation (S_{dev}) for the grain size and the t/d ratio.

Table 1
Example of six heat treatment conditions (time = 220 min) and the corresponding mean grain size, standard deviation for the mean grain size and the number of grains across the thickness.

Temperature (K)	Grain size (μm)	S_{dev} (μm)	t/d
873	40	25	12.5
1073	83	45	6.1
1123	130	76	3.8
1198	160	90	3.1
1223	200	119	2.5
1323	500	244	1

Quantitative texture analysis was followed as a function of the mean grain size using neutron diffraction. Measurements were carried out using the eulerian cradle of the D1B instrument at the ILL reactor (Grenoble-France). Full diagrams in the 20–100 2θ range were acquired using the curved position sensitive detector, for the 1368 sample orientations corresponding to a regular $5^\circ \times 5^\circ$ texture grid in χ and φ. Each diagram was measured for 4 s at a $\lambda = 0.2523$ nm wavelength. Neutron diffraction was used rather than X-ray diffraction as the number of probed grains is higher (around 30,000 grains for the largest mean grain size with neutron diffraction vs. 300 with X-ray diffraction). Nickel samples for neutron diffraction were prepared by gluing 1 cm × 1 cm plates from the original specimens in order to obtain 1 cm edge cubes. During this step, the main rolling directions were kept parallel between square slabs. The orientation distribution function (ODF) was refined using the E-WIMV algorithm from LeBail extracted pole figures within the combined analysis formalism [31] as implemented in the Maud software [32]. The ODF was used to reconstruct normalised main pole figures and are expressed in multiples of a random distribution (m.r.d. unit). The {1 1 1}, {2 0 0} and {2 2 0} recalculated pole figures for three different grain sizes are given in Fig. 1. For all specimens, the crystallographic texture looks similar with a maximal density lower than 2 m.r.d.

The macroscopic stiffness tensor of the samples was calculated from the ODF using the geometric approach [33] using Beartex software [34]. The stiffness tensor of the single crystal used in the calculation was: $C_{11} = C_{22} = C_{33} = 248$ GPa; $C_{12} = C_{13} = C_{23} = 153$ GPa; $C_{44} = C_{55} = C_{66} = 116$ GPa [35]. Table 2 reports the stiffness tensor components of the sample for five grain sizes.

Despite a difference in the number of grains across the thickness, the components of the macroscopic stiffness tensor are rather con-

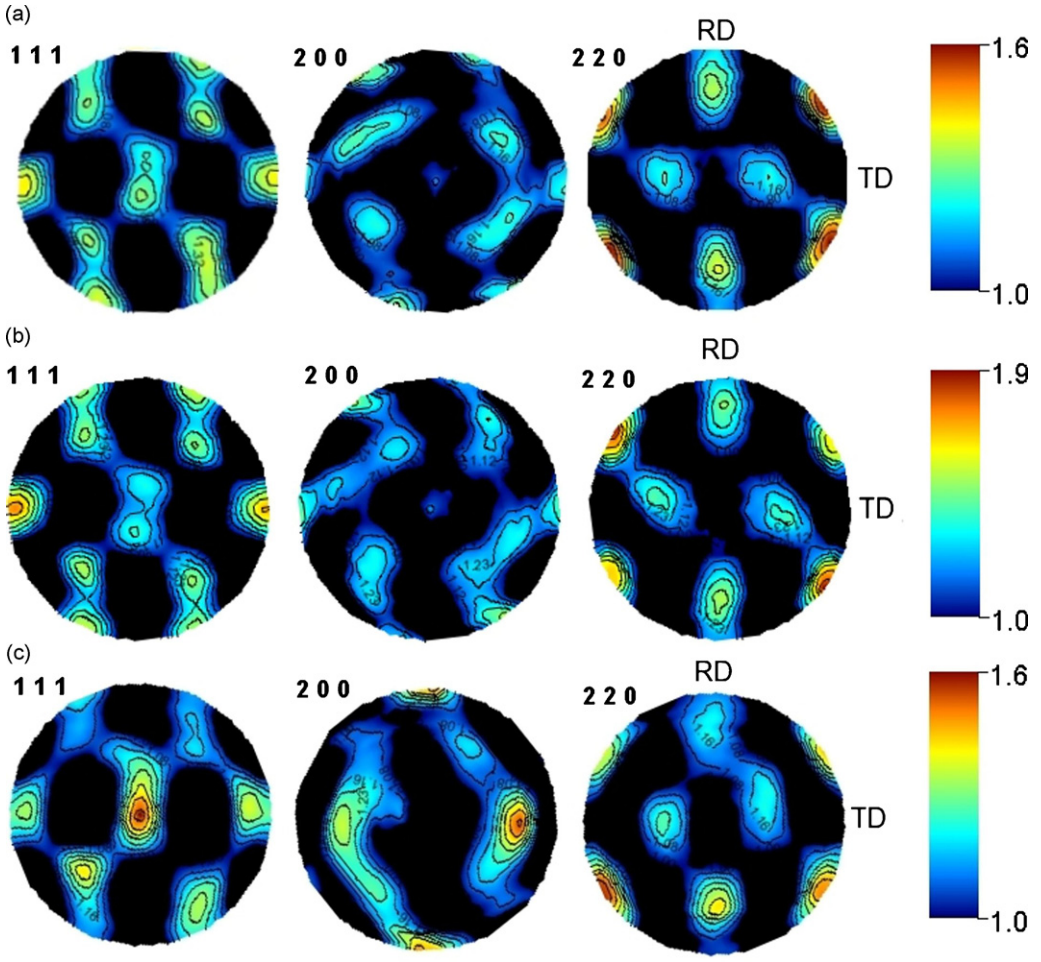

Fig. 1. Normalised {1 1 1}, {2 0 0} and {2 2 0} pole figures for three samples: (a) $d = 40\ \mu m$; (b) $d = 120\ \mu m$; (c) $d = 220\ \mu m$; recalculated from neutron diffraction datas.

stant. Table 3 gives the Young (E) and shear modulus (μ), Poisson's ratio (ν) and the elastic anisotropy coefficient ($A = 2C_{44}/(C_{11} - C_{12})$) calculated from the macroscopic stiffness tensor with the cubic symmetry assumption for five grain sizes.

The elastic properties of the five samples are constant, in accordance with the experimental values found for nickel. Moreover all the samples are isotropic as A is close to unity (A is equal to 2.5 for nickel single crystal). The crystallographic texture is therefore assumed not to be affected by grain size variation as already reported for copper polycrystals in [36]. The weak difference of pole figures and maximal density pole between the specimens is expected to have no influence on the mechanical properties as the macroscopic stiffness tensor and elastic properties are constant. These results show that unstrained surface grains and core grains (respectively, mainly analysed for samples of 200 μm and 40 μm grain size) have the same crystallographic orientation. Consequently, the same Schmid factors can be expected wherever the location of the grain in the sample and thus the same strengthening behaviour. No size effect due to a difference between the crystallographic texture of the core and the surface grains can take place as reported in Ref. [28].

Grain boundary character distribution was also studied in order to measure the proportion of low-Σ CSL (coincident site lattice) boundaries. The fraction of the latter and especially the Σ_3 boundaries was found to modify the mechanical properties of Ni and Fe-based alloys [37,38]. The fraction of Σ_3, Σ_9 and random grain boundaries was studied by EBSD on a scanning electron microscope using the TexSem laboratory software. Fig. 2 shows the fraction of

Table 3
Mean grain size and elastic properties for five samples.

Grain size (μm)	μ (GPa)	E (GPa)	ν	A
40	81.27	212.50	0.31	1.01
80	80.78	211.62	0.31	1.00
120	80.53	211.12	0.31	0.99
160	80.64	211.33	0.31	0.99
220	80.26	210.62	0.31	0.98

Table 2
Mean grain size and macroscopic stiffness tensor for five samples.

Grain size (μm)	$C_{11} = C_{22} = C_{33}$ (GPa)	$C_{12} = C_{13} = C_{23}$ (GPa)	$C_{44} = C_{55} = C_{66}$ (GPa)	Others components (GPa)
40	292.67	130.66	81.28	0.02
80	293.64	130.17	80.78	−0.01
120	294.17	129.92	80.53	−0.05
160	293.95	130.02	80.64	−0.10
220	294.76	129.61	80.27	−0.06

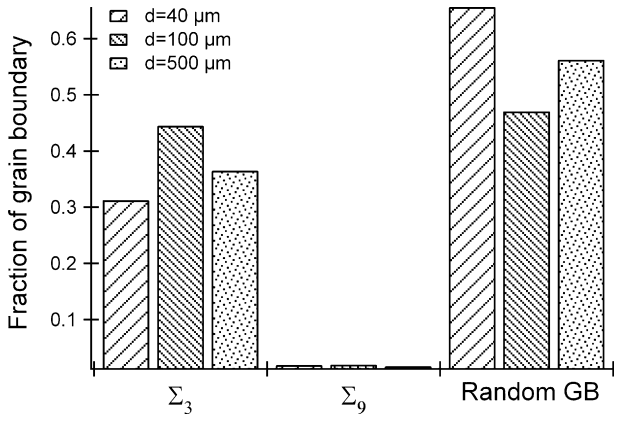

Fig. 2. Fraction of Σ_3, Σ_9 and random grain boundaries for three grain sizes measured by EBSD.

the three grain boundaries for three grain sizes for unstrained samples. The "random" and Σ_3 boundaries are the major components while Σ_9 boundaries are for all purpose absent. However, there is no evidence of correlation between the grain size and the proportion of low-Σ CSL.

2.3. Tensile test description

The overall mechanical behaviour of the samples was first characterized in monotonous tensile conditions. The test was strain rate controlled at a strain rate of $2.4 \times 10^{-4}\,s^{-1}$ and the strain measurement was achieved by a classical extensometer mounted directly on the gauge section of the samples. A total of 80 tensile tests were carried out. Experimental standard deviation was estimated on 45 experimental tensile tests among them.

Loading/unloading tensile tests were then carried out in order to study the effect of the t/d ratio on strengthening. The flow stress can be divided into two parts according to Dickson et al. [39], namely the effective stress (σ_{eff}) and the backstress (X). Physically, the backstress is linked to the local straining process which introduces long-range interactions with mobile dislocations (i.e., grain boundaries, dislocation cells, etc.). The backstress is a directional component of hardening. The effective stress, which is an isotropic component of hardening, represents the stress locally required for a dislocation under short-range interaction to move (i.e., dislocation forest interactions, coherent precipitates, etc.) [40].

These components can be obtained by studying the hysteresis loops created during the loading/unloading tests. Fig. 3 represents the details of one unload/load sequence extracted from a global

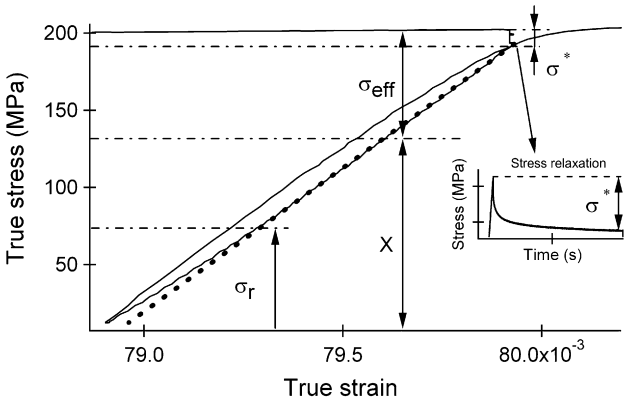

Fig. 3. Flow stress partition during unloading.

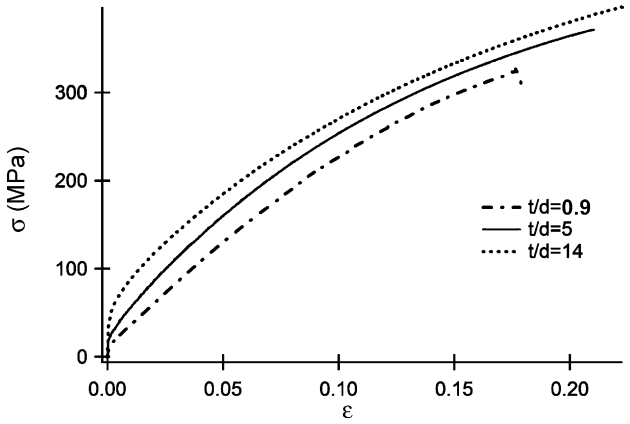

Fig. 4. Typical stress–strain curves for three specimens: $t/d = 0.9$, 5 and 14.

unloading/loading stress–strain curve. The stress partition can be expressed by the following relations [40]:

$$\sigma_{eff} = \frac{\sigma - \sigma_r}{2} + \frac{\sigma^*}{2} \quad (1)$$

$$X = \sigma - \sigma_{eff} \quad (2)$$

with σ_r the reverse yield stress and σ^* the thermally activated part of the effective stress. The most important factor to make this stress partition reliable is a high unloading speed acting as a mechanic quench which prevents a reorganization of the dislocation structures. σ^* was obtained thanks to stress relaxation reaching a stabilization of the σ^* value with time before unloading (see Fig. 3). However, the determination of the two components of the flow stress by loading/unloading tests is quite difficult. The value of X and σ_{eff} are thus given with an accuracy of 10%.

3. Mechanical results

3.1. Effect of the t/d ratio on the hardening behaviour

Fig. 4 shows the typical stress–strain curves of a tensile test for three samples with different t/d ratios: 0.9, 5 and 14. These three samples represent, respectively a low, an intermediate and a high t/d ratio specimen. The difference of flow stress level between the three specimens is due to both grain size and t/d ratio effects.

For metallic samples, strain hardening results from the evolution of the dislocation density with strain. According to previous works, the stress can be classically written as a function of the dislocation density ρ [41,42]:

$$\sigma = M\alpha\mu b\sqrt{\rho} \quad (3)$$

here, M is the Taylor factor, b is the Burger's vector, μ is the shear modulus and α is a material parameter taking into account the dislocation arrangement. The evolution rate of the dislocation density with strain has been described as being composed of two main parts [42–44]:

$$\frac{d\rho}{d\varepsilon} = \frac{M\sqrt{\rho}}{\beta b} - \frac{2MPy\rho}{b} \quad (4)$$

The first term of the right hand side is related to the athermal storage of mobile dislocations which become immobilized after having travelled a distance proportional to the average slip spacing. The second term is associated with the annihilation of dislocations due to cross-slip during dynamic recovery [43,45]. β represents the ratio between the mean free path of gliding dislocations and the average dislocation distance and P is a probability that two dislocations annihilate each other when they are separated by a distance

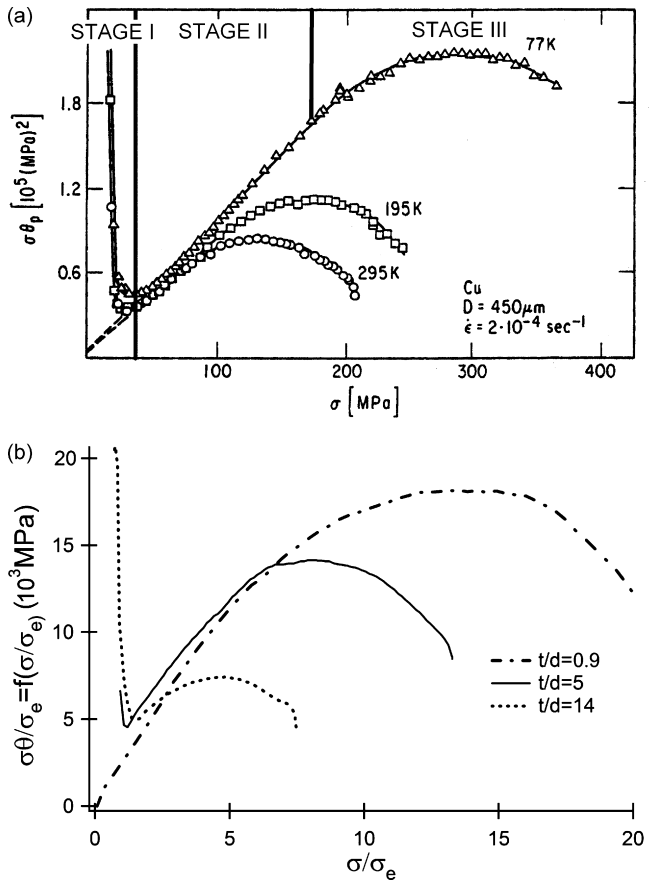

Fig. 5. (a) Evolution of the relation $\sigma\theta$ vs. σ for Cu polycrystals for three temperatures [41] and (b) evolution of the relation $\sigma\theta$ vs. σ for three nickel polycrystals with 0.9, 5 and 14 grains across the thickness. All the stresses are normalized by the yield stress σ_e.

y. The value of this annihilation distance can be obtained by TEM investigations [43].

Combining Eqs. (3) and (4), the product $\sigma d\sigma/d\varepsilon$ can be expressed as

$$\sigma\frac{d\sigma}{d\varepsilon} = \frac{\alpha\mu M^2}{2\beta}\sigma + f(\sigma, P, y, \rho) \quad (5)$$

The second term of the right hand side of Eq. (5) is present with the activation of cross-slip in the material.

The plot of $\sigma\theta$ with $\theta = d\sigma/d\varepsilon$ as a function of stress is therefore suitable to study the different hardening stages of polycrystalline samples [41]. Fig. 5(a) represents a plot of $\sigma\theta$ vs. σ for a copper polycrystal for three temperatures (from Ref. [41]). The three common hardening stages for polycrystals are exhibited for 77 K. Stage I corresponds to microplasticity. During this stage, plasticity is established from grain to grain until a homogeneous state is reached. The second stage is characterised by a linear variation of $\sigma\theta$ as the second term in Eq. (5) disappears (during stage II, cross-slip is expected to have a reduced activity [41,45]). The third stage begins with a deviation from the linearity portion of the curve due to the negative contribution on strain hardening of the dynamic recovery.

Fig. 5(b) shows the $\sigma\theta$ vs. σ curves for the three Ni samples with $t/d = 0.9$, 5 and 14. In order to compare the length of the stages between the three specimens, all stress values were normalised by the yield stress σ_e (stress for $\varepsilon = 0.002$) of each sample. For $t/d = 5$ and 14, the second stage is reached approximately within the yield stress. For $t/d = 1$, as the number of grains is reduced compared to the other samples, the homogenisation of plasticity is faster. Experimentally, stage I is therefore difficult to visualise in Fig. 5(b) and the second stage is reached for lower stress.

Fig. 6(a and b) shows, respectively the strain length $\Delta\varepsilon_{II}$ (strain range for which stage II occurs) and the hardening rate θ_{II} of the second stage vs. the t/d ratio.

As seen in Fig. 6(a), the second stage adopts asymptotic behaviour for the samples with more than four grains across the thickness as no linear portion of the curve has been found. For specimens with less than four grains across the thickness, the length of the second stage increases with a decrease of t/d. For the sample with only one grain across the thickness, the second stage reaches a length $\Delta\varepsilon_{II}$ of 3%.

The hardening rate in stage II (Fig. 6(b)) slightly decreases with t/d. This results from the grain size effect as previously reported by Feaugas and Haddou [40]. For specimens with t/d higher than 4, the hardening rate was taken as being equal to the slope of the asymptote of the curve $\sigma\theta$ vs. σ after the first stage. The mean value for θ_{II} is around 2100 MPa. This value is around half the value of $\mu/200$ in resolved shear stress and strain found for single crystals (dividing θ_{II} by M^2 with a value for M, the Taylor factor, of 3 found by EBSD analysis). This value is in agreement with the usual value reported for polycrystals ($\mu/200$) [42,44].

3.2. Hall and Petch behaviour

In order to differentiate the grain size effect and the t/d ratio effect from the overall size effect seen in Fig. 4,σ, σ_{eff} and X have been plotted as a function of the inverse of the square root of the grain size. The well known Hall and Petch (HP) formulation originally describes the grain size dependence on the stress and has been extended for higher strain levels [17,40,42,46]:

$$\sigma(\varepsilon) = \sigma_0(\varepsilon) + \frac{k_{hp}(\varepsilon)}{\sqrt{d}} \quad (6)$$

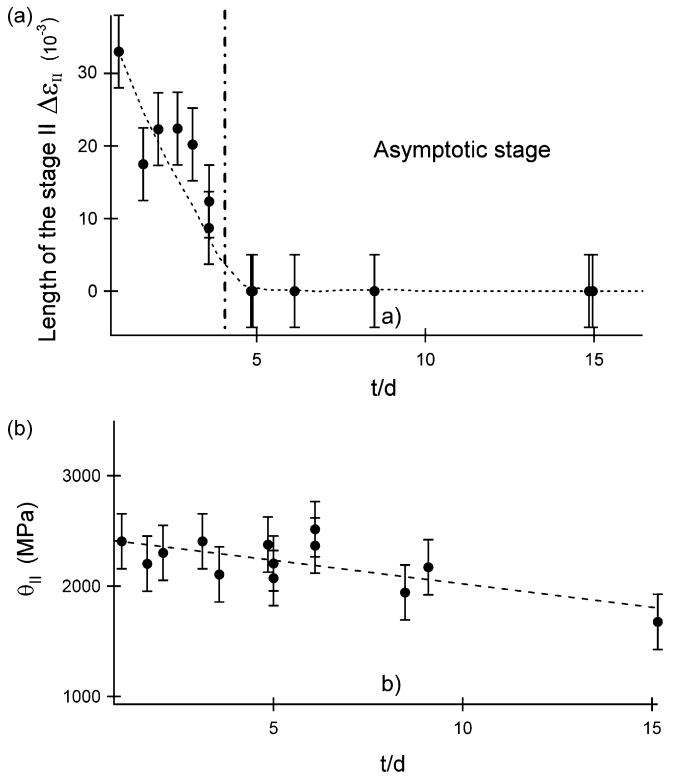

Fig. 6. (a) Evolution of the strain length of the second hardening stage and (b) evolution of the hardening rate θ_{II} of the second stage vs. t/d.

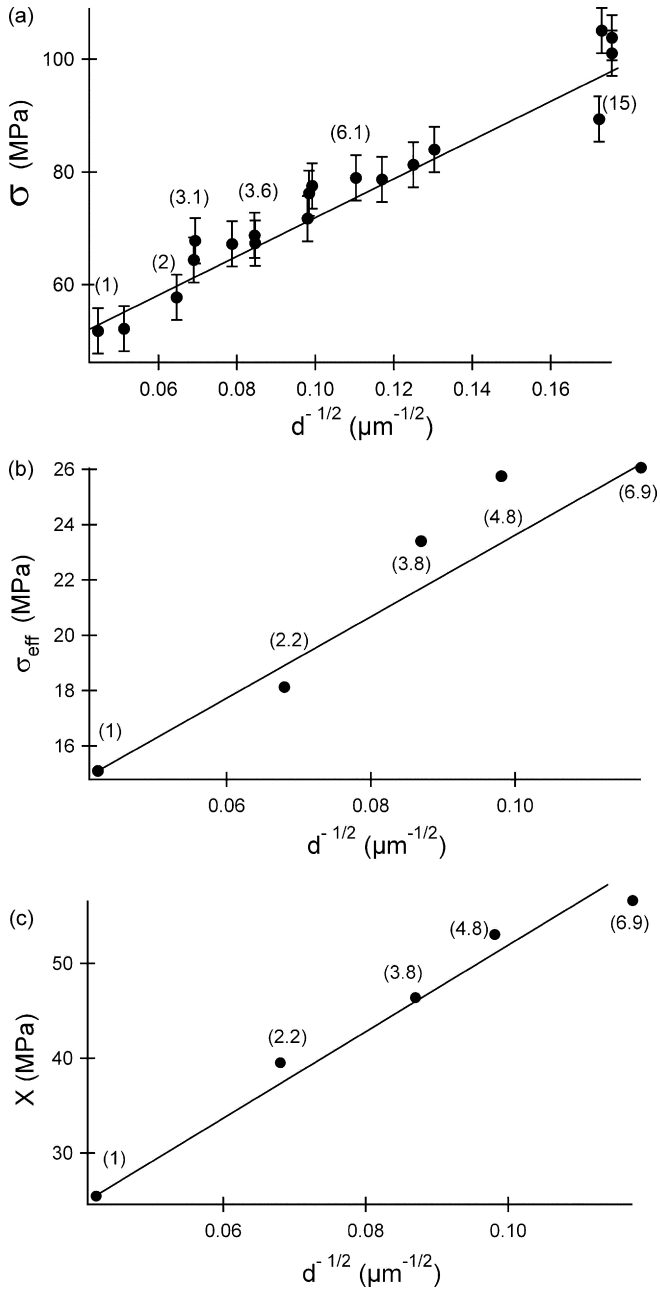

Fig. 7. Hall–Petch relation for a strain of 0.015 applied to (a) σ, (b) σ_{eff} and (c) X. Specimen t/d ratio is represented in brackets.

where $\sigma_0(\varepsilon)$ and $k_{hp}(\varepsilon)$ are material empirical constants which depend on strain. This relationship was found to represent correctly the grain size dependence of the effective stress and long-range backstress for nickel and stainless-steel AISI 316 L [40]:

$$X(\varepsilon) = X_{intra}(\varepsilon) + X_{inter}(\varepsilon) = X_0(\varepsilon) + \frac{k_X(\varepsilon)}{\sqrt{d}} \quad (7)$$

$$\sigma_{eff}(\varepsilon) = \sigma_{eff_0}(\varepsilon) + \frac{k_{eff}(\varepsilon)}{\sqrt{d}} \quad (8)$$

The application of the HP law split the backstress into two components: the intragranular backstress $X_{intra} = X_0(\varepsilon)$ and the intergranular one $X_{inter} = k_X(\varepsilon)/\sqrt{d}$. The intragranular backstress is linked to the dislocation structures in the grains while the intergranular backstress is related to the strain incompatibilities between the different grains. X_{inter} is grain size dependent in opposition to X_{intra} which is, at first glance, not sensitive to the grain size [40].

The application of the relations (6), (7) and (8) for strains of 0.015 and 0.08 is presented, respectively in Figs. 7(a) and 8(a) for σ, Figs. 7(b) and 8(b) for σ_{eff} and Figs. 7(c) and 8(c) for X.

For a strain of 0.015 (Fig. 7), the HP relation represents correctly the grain size dependence of the stress components. The overall size effect seen for this amount of strain is therefore dominated by the grain size effect. For a strain of 0.08 (Fig. 8), σ exhibits two distinct stages, delimited by a t/d ratio of 3.3. The presence of these two stages for the flow stress has been found to result from a t/d ratio effect [22]. As shown in Fig. 8(b), σ_{eff} is unambiguously unchanged by a decrease of t/d as no different slopes appear. As the effective stress is not affected by a variation of the number of grains across the thickness, the decrease of the flow stress σ must be caused by a decrease of the long-range backstress. Despite the presence of only a few experimental points, this feature is confirmed by the examination of Fig. 8(c) which shows a decrease of the backstress

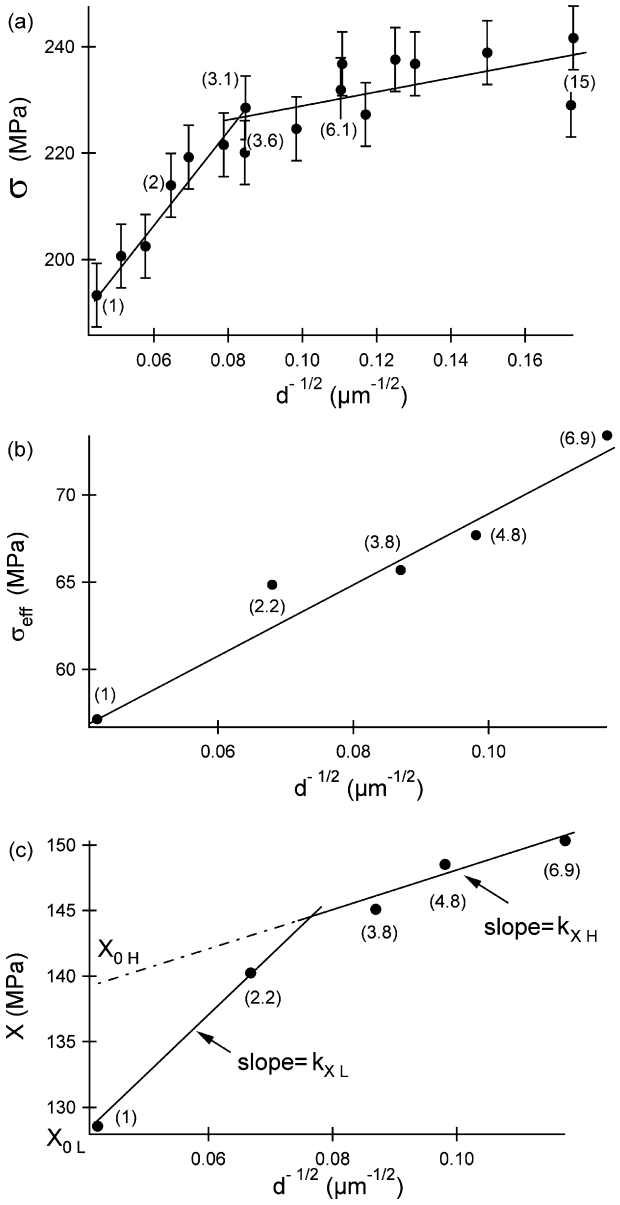

Fig. 8. Hall–Petch relation for a strain of 0.08 applied to (a) σ, (b) σ_{eff} and (c) X. Specimen t/d ratio is represented in brackets.

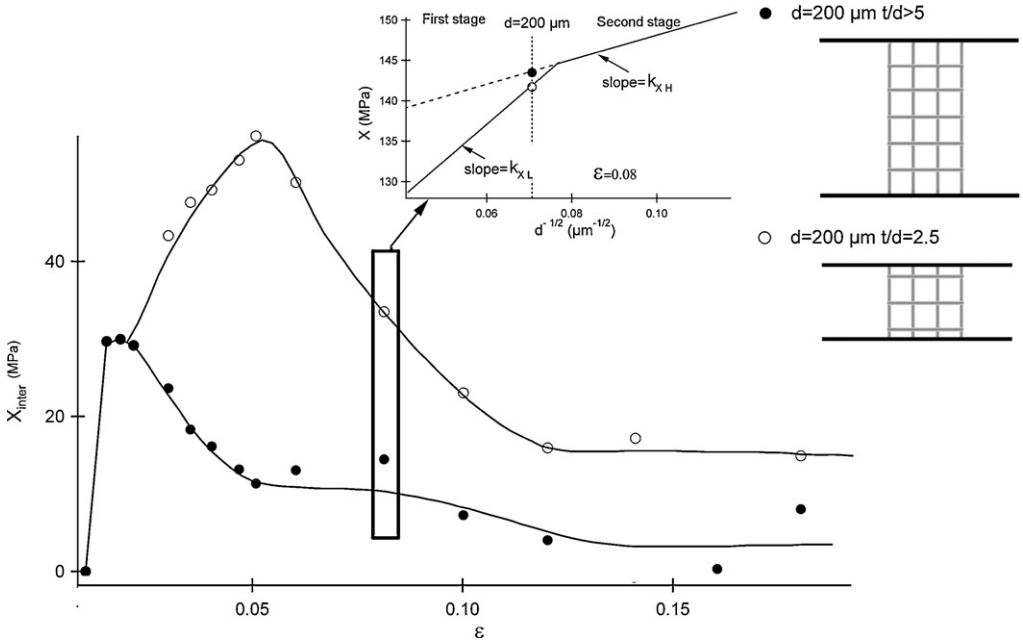

Fig. 9. Evolution of the intergranular backstress with strain for two 200 μm grain size samples, one $t/d = 2.5$ (open circles) and the other for $t/d > 5$ (plain circles). X_{inter} was computed using Eq. (7) and HP plots as Figs. 7(c) and 8(c) for strains ranging between 0 and 0.18.

for specimens with less than around three grains across the thickness. For samples with a t/d ratio lower than 3, the intragranular part of the backstress X_0 is lower (X_{0L}) than for higher t/d ratio specimens (X_{0H}). Bearing in mind that $X_{inter} = k_X(\varepsilon)/\sqrt{d}$, the intergranular part of the backstress is also increased as the slope of Fig. 8(c) (k_X) increases with a decrease of t/d.

4. Discussion

With a reduction of the t/d ratio, both the hardening stages and backstress are modified in polycrystalline nickel. This modification appears when the number of grains across the thickness is lower than a critical value which depends, for Ni, on the amount of strain as previously reported [22].

Despite numerous studies dedicated to the specimen size effect, the mechanisms associated with the t/d ratio effect remains unclear. In a recent work, Janssen et al. emphasize that the overall change of the mechanical behaviour could be due to a variation of the microstructure like crystallographic texture or oxide layer formation with a reduction of the t/d ratio [18]. The microstructure and texture for our samples are very similar as no significant change in the crystallographic texture, elastic properties and grain boundary character distribution was found when the t/d ratio became lower than 4. Other mechanisms are thus responsible for the modification of the mechanical properties.

For Al and Cu single crystals with no oxide layer on the surfaces, the presence of a stress gradient between the surface and the core of the specimen was reported [1–7]. This gradient was attributed to the escape of primary dislocations through the free surfaces. Consequently, the dislocation density near the free surfaces is lower and the formation of heterogeneous dislocation structures is delayed compared to the core of the sample [1–5]. For a single crystal oriented for single glide, strained up to 0.05, it was shown that the surface region deforms in stage I in single glide, while the core region deforms in stage II with multiple slip. Macroscopically, this difference in the hardening stages between the surface and core regions results in a modification of the strain range for the first and second hardening stages with a decrease of the specimen dimensions [1,7]. As the dimensions are reduced, the surface region becomes dominant over the core region.

The increase in the strain length of the second hardening stage for Ni with a decrease of t/d (Fig. 6(a)) below the critical value suggests similar mechanisms.

The hardening stages for fcc metallic polycrystals are related to the activated gliding systems in the material. The first stage is characterised by the activation of primary $\{1\,1\,1\}\ \langle 1\,1\,0\rangle$ gliding systems. The second stage is generally associated with the activation of primary and secondary systems and a few cross-slips [40,45]. The multiple gliding systems induce the formation of heterogeneous dislocation structures like tangles, walls or cells. These structures are responsible for an increase in the intragranular backstress. The third stage is related to the generalization of cross-slip in the material and the dominance of dislocation cells in the grains. During the second and the third stages, the activation of cross-slip reduces the intergranular backstress as reported in [40].

The delay of the activation of the third hardening stage for the low t/d ratio Ni polycrystals could result from the hold of the generalization of the cross-slip activity in the material. Fig. 9 confirms this mechanism. This figure shows the evolution of the intergranular backstress with strain for two samples with a mean grain size of 200 μm but with low and high t/d ratio values. This plot was constructed by the examination of the k_X coefficients ($X_{inter} = k_X(\varepsilon)/\sqrt{d}$) of the Hall–Petch plots for the backstress for strains between 0.01 and 0.18.

The first curve (open circles) is derived from the slope of the first stage of the backstress HP plot (k_{XL}) for a sample with 2.5 grains across the thickness and a total thickness of 0.5 mm. The second curve (plain circles) derives from the slope of the second stage of the backstress HP plot (k_{XH}) extrapolated for the higher grain sizes as no samples with large grain sizes and high t/d ratios were tested. This extrapolation for Ni is valid if the t/d ratio is higher than the critical value [46]. The second sample is then assumed to have more than five grains across the thickness.

For a strain higher than 0.02, the intergranular backstress of the thicker sample is relaxed by the generalization of cross-slip. For the thinner sample, X_{inter} still increases for strains up to 0.05 and then

decreases. This strain hold of 0.03 for the generalization of cross-slip for the thinner sample is in agreement with the difference in strain length of the second hardening stage between a sample with $t/d = 2.5$ and a sample with $t/d > 5$ (Fig. 6(a)).

Furthermore, the t/d ratio also affects the intragranular backstress. As cross-slip is activated later, the formation of heterogeneous dislocation structures for the lower t/d ratio samples is supposed to be delayed compared with the high t/d ratio specimens. The intragranular backstress, X_{intra}, is then reduced [47] for the lowest t/d ratio specimens, as shown in Fig. 8(c).

This decrease of intragranular backstress is in accordance with previous TEM and etching investigations of dislocation structures on core and surface grains of Cu and Ni solicited in uniaxial tension [13,16], and HSLA steel polycrystals loaded in low cycle fatigue [48]. It was reported that the dislocation arrangement is more heterogeneous for core grains than for surface grains. This difference of dislocation structures between surface and core grains involves a modification of intragranular backstress. As the number of grains across the thickness is reduced, the surface grains are predominant and the intragranular backstress of the entire sample decreases. This change of the magnitude of the flow stress for low t/d ratio specimens is therefore due to the loss of intragranular backstress, as this component of the backstress is dominant for strains larger than a few percent.

Nevertheless, the origin of the cross-slip delay remains unknown. Several authors conclude from TEM investigations or numerical simulations that in polycrystals, surface grains accommodate strain by single glide for a longer time than core grains [9,48,49]. The activation of multiple and cross-slip is hence delayed for surface grains. These features were attributed to the presence of free surfaces. The delay in the generalization of cross-slip found experimentally for nickel samples with a few grains across the thickness seems to result from the surface effects. Despite a relatively high thickness (0.5 mm), nickel samples are sensitive to the presence of free surfaces when less than approximately four grains across the thickness are present.

This mechanism is in agreement with Janssen et al. who assessed for Al specimens with few grains across the thickness that the stress decrease is due to a reduction of the proportion of horizontal grain boundaries [18]. As all microstructural aspects are constant for the different Ni samples, only the variation of the proportion of the horizontal grain boundaries can be responsible for the behaviour modification. This kind of grain boundaries may prevent the extension of surface effect in the core regions of the material.

In order to confirm this mechanism of the modification of hardening behaviour, TEM investigations of dislocation structures in nickel as a function of the t/d ratio and the distance to the free surface are in progress. The objective is to confirm the difference of intragranular and intergranular backstress between low and high t/d ratio specimens by studying the heterogeneous dislocation structures.

5. Conclusion

A physical mechanism is proposed to explain the modification of the mechanical properties of Ni polycrystalline samples with few grains across the thickness. Following microstructural studies and experimental results on uniaxial and loading/unloading tensile tests, a reduction of the t/d ratio below the critical value induces the following features:

1. The initial microstructure of nickel samples is not modified. Crystallographic texture, elastic properties and grain boundary character distribution remain insignificantly unchanged.
2. A linear hardening stage (stage II) appears on the strengthening curves of the material. The strain length of this stage increases with a decrease in t/d.
3. The intragranular backstress, related to the heterogeneous dislocations structures, decreases. The intergranular part of the backstress increases.

These features can be explained by a delay of the generalization of cross-slip due to surface effects for specimens with few grains across the thickness. The decrease of stress generally found with a reduction of the number of grains across the thickness is therefore mainly due to a reduction of intragranular backstress. The evolution of the critical t/d ratio with strain can be also explained by the cross-slip delay. These results are of prime interest for rolled thin films, widely used for micro-components, which generally have few grains across the thickness.

Acknowledgments

The authors express their thanks to Mr. B. Ouladdiaf and F. Leon from the ILL-Grenoble, France, for their technical and scientific help with neutron diffraction. C. Keller greatly acknowledges the "Conseil Régional de Basse-Normandie, France" for its PhD financial support.

References

[1] J.T. Fourie, Phil. Mag. 15 (1968) 735–756.
[2] J.T. Fourie, N.C.G. Dent, Acta Metall. 20 (1972) 1291–1296.
[3] J.T. Fourie, Phil. Mag. 21 (1970) 977–985.
[4] H. Mughrabi, Phys. Stat. Sol. (B) 44 (1971) 391–402.
[5] H. Mughrabi, Phys. Stat. Sol. (B) 39 (1970) 317–327.
[6] Z. S. Basinski: in Surface effects in crystal plasticity, R.M. Latanision and J.T. Fourie, Nato Advanced Study Institutes Series, 1977, pp. 433–467.
[7] H. Suzuki, S. Ikeda, S. Takeushi, J. Phys. Soc. Jpn. 11 (1956) 382–393.
[8] I.R. Kramer, Trans. Met. Soc. AIME 227 (1963) 1003–1010.
[9] J.T. Fourie, Strength of Metals and Alloys proceeding of the 7th International Conference, Pergamon Press, 1977, pp. 99–104.
[10] P.R. Swann, Acta Metall. 14 (1966) 900–903.
[11] K. Sumino, M. Yamamoto, Acta Metall. 11 (1963) 1223–1234.
[12] K. Sumino, Y. Kawasaki, M. Yamamoto, M.P. Sumino, Acta Metall. 11 (1963) 1235–1243.
[13] K. Kolb, E. Macherauch, Phil. Mag. 7 (1961) 415–426.
[14] R.W. Armstrong, J. Mech. Phys. Solids 9 (1961) 196–199.
[15] A.W. Thompson, Scripta Metall. 8 (1973) 145–148.
[16] S. Miyazaki, K. Shibata, H. Fujita, Acta Metall. 27 (1979) 855–862.
[17] N. Hansen, Acta Metall. 25 (1977) 863–869.
[18] P.J.M. Janssen, Th.H. de Keijser, M.G.D. Geers, Mater. Sci. Eng. A 419 (2006) 238–248.
[19] G. Simons, Ch. Weippert, J. Dual, J. Villain, Mater. Sci. Eng. A 416 (2006) 290–299.
[20] G.P.K. Jun Ni, M. Koç, Trans. ASME. 129 (2007) 470–476.
[21] M. Henning, H. Vehoff, Mater. Sci. Eng. A 452–453 (2007) 602–613.
[22] C. Keller, E. Hug, Mater. Lett. 62 (2008) 1718–1720.
[23] T.A. Kals, R. Eckstein, J. Mater. Process. Technol. 103 (2000) 95–101.
[24] L.V. Raulea, A.M. Goijaerts, L.E. Govaert, F.P.T. Baaijens, J. Mater. Process. Technol. 115 (2001) 44–48.
[25] J.F. Michel, P. Picart, J. Mater. Process. Technol. 141 (2003) 439–446.
[26] J.T. Gau, C. Principe, J. Wang, J. Mater. Process. Technol. 184 (2007) 42–46.
[27] T. Fulöp, W.A.M. Brekelmans, M.G.D. Geers, J. Mater. Process. Technol. 174 (2006) 233–238.
[28] S. Nemat-Nasser, A. Maximenko, E. Olevsky, J. Mech. Phys. Solids 54 (2006) 2474–2494.
[29] P.J.M. Janssen, J.P.M. Hoefnagels, Th.H. de Keijser, M.G.D. Geers, J. Mech. Phys. Solids 56 (2008) 2687–2706.
[30] S. Berbenni, V. Favier, M. Berveiller, Int. J. Plast. 23 (2007) 114–142.
[31] D. Chateigner, Combined analisys: structure, texture, microstructrure, phase, stresses-reflectivity determination by X-ray and neutrons scattering, http://www.ecole.ensicaen.fr/~chateign/texture/combined.pdf.
[32] L. Lutterotti, S. Matthies, H.R. Wenk, MAUD (Material Analysis Using Diffraction): a user friendly Java program for Rietveld texture analysis and more, National Research Council of Canada, Ottawa, 1999, pp. 1599–1604.
[33] S. Matthies, M. Humbert, J. Appl. Crystallogr. 28 (1995) 254–266.
[34] H.R. Wenk, S. Matthies, J. Donovan, D. Chateigner, J. Appl. Crystallogr. 31 (1998) 262–269.
[35] K.H. Hellwege (Ed.), Landolt-Börnstein tables, new series, group III, Springer-Verlag, New-York, 1 (1966) p.6.

[36] D. Juul Jensen, A.W. Thompson, N. Hansen, Metall. Mater. Trans. 20A (1989) 2803–2809.
[37] P. Lin, G. Palumbo, U. Erb, K.T. Aust, Scripta Metall. Mater. 33 (1995) 1387–1392.
[38] L. Tan, K. Sridharan, T.R. Allen, R.K. Nanstad, D.A. McClintok, J. Nucl. Mater. 374 (2008) 270–280.
[39] J.I. Dickson, J. Boutin, L. Handfield, Mater. Sci. Eng. 64 (1984) L7–L11.
[40] X. Feaugas, H. Haddou, Metal. Trans. 34A (2003) 2329–2340.
[41] H. Mecking, in: A.W. Thompson (Ed.), Work Hardening in Tension and Fatigue, TMS-AIME, New York, 1977, pp. 67–89.
[42] H. Mecking, U.F. Kocks, Acta Metall. 29 (1981) 1865–1875.
[43] U. Essmann, H. Mughrabi, Phil. Mag. A 40 (1979) 731–756.
[44] T. Narutani, J. Takamura, Acta Metall. 39 (1991) 2037–2049.
[45] J.E. Flinn, D.P. Field, G.E. Korth, T.M. Lillo, J. Macheret, Acta Mater. 49 (2001) 2065–2074.
[46] A.W. Thompson, in: A.W. Thompson (Ed.), Work Hardening in Tension and Fatigue, TMS-AIME, New York, 1977, pp. 89–126.
[47] H. Mughrabi, Acta Metall. 31 (1983) 1367–1379.
[48] R. Keller, W. Zielinski, W.W. Gerberich, Mater. Sci. Eng. A 113 (1989) 267–280.
[49] M. Sauzay, P. Gilormini, C. R. Acad. Sci. Paris, Series II b 328 (2000) 117–122.